Bioinspired Nanocomposites

Deutsche Ausgabe: DOI: 10.1002/ange.201502323
Internationale Ausgabe: DOI: 10.1002/anie.201502323

Hierarchical Nacre Mimetics with Synergistic Mechanical Properties by Control of Molecular Interactions in Self-Healing Polymers**

*Baolei Zhu, Nils Jasinski, Alejandro Benitez, Manuel Noack, Daesung Park, Anja S. Goldmann, Christopher Barner-Kowollik, and Andreas Walther**

Abstract: *Designing the reversible interactions of biopolymers remains a grand challenge for an integral mimicry of mechanically superior biological composites. Yet, they are the key to synergistic combinations of stiffness and toughness by providing sacrificial bonds with hidden length scales. To address this challenge, dynamic polymers were designed with low glass-transition temperature T_g and bonded by quadruple hydrogen-bonding motifs, and subsequently assembled with high-aspect-ratio synthetic nanoclays to generate nacre-mimetic films. The high dynamics and self-healing of the polymers render transparent films with a near-perfectly aligned structure. Varying the polymer composition allows molecular control over the mechanical properties up to very stiff and very strong films ($E \approx 45$ GPa, $\sigma_{UTS} \approx 270$ MPa). Stable crack propagation and multiple toughening mechanisms occur in situations of balanced dynamics, enabling synergistic combinations of stiffness and toughness. Excellent gas barrier properties complement the multifunctional property profile.*

In the last decade, the nacreous layer of mollusks has received enormous attention for its extraordinary combination of stiffness, toughness, and strength.[1] Nacre contains 95 vol% aragonite microtablets, which are laminated by a complex matrix of biopolymers containing silk fibroins, chitin nanofibrils, and a range of fusion proteins in a brick-and-mortar architecture. The structure of the soft part guides the layered growth, and provides toughness by plastic deformation, frictional sliding and molecular energy-dissipation (for example, unfolding of secondary motifs).

Such natural high-performance materials inspire synthetic bioinspired nanocomposites (NCs). Those contrast traditional NCs, by aiming at highly ordered structures at high levels of reinforcements, and at best mimicking the complexity of the natural biopolymers with molecularly controlled strengthening and energy-dissipation mechanisms.

There has been a range of approaches to mimic nacre,[1d] most notably sequential deposition of platelets and polymers,[2] or ice templating and sintering of ceramics, followed by resin infusion.[3] We developed a very efficient colloidal pathway to mimic the brick-and-mortar structure by self-assembly of polymer-coated (core–shell) nanoclay platelets.[4] This approach is energy-efficient at room temperature, benign due to aqueous processing, and scalable to large dimensions.[5]

Most efforts to tailor the properties in nacre mimetics by the soft phase are still based on commercial polymers with high glass-transition temperature (T_g), and post-infiltration of covalent and ionic cross-linking agents.[2–6] However, such interactions are very strong and show little dynamics at ambient conditions, hence failing to address a balance of stiffening with stress-induced opening/rebinding needed to create toughness.[7] Surprisingly, no efforts have so far been made to use sophisticated macromolecular engineering to impart advanced polymer characteristics such as hydrogen-bonding mediated self-healing or other reversible bonding scenarios into nacre-mimetic NCs by careful design of the polymer building blocks. This would however open versatile avenues towards the rational design of the soft phase, and allow targeting synergetic increases in stiffness and toughness. This particularly involves the engineering of sacrificial bonds via stick/slip interactions or unfolding of secondary motifs, which are highly sought after in bioinspired materials design.[7]

Our understanding of reversible polymers based on supramolecular or dynamic covalent interactions has revolutionized polymer science by providing self-healing materials.[8] These can be distinguished in autonomously self-healing materials, commonly found in elastomers with low T_g and

[*] B. Zhu, A. Benitez, M. Noack, Dr. A. Walther
DWI—Leibniz-Institute for Interactive Materials
Forckenbeckstrasse 50, 52056 Aachen (Germany)
E-mail: walther@dwi.rwth-aachen.de
Homepage: http://www.dwi.rwth-aachen.de
N. Jasinski, Dr. A. S. Goldmann, Prof. Dr. C. Barner-Kowollik
Preparative Macromolecular Chemistry
Institut für Technische Chemie und Polymerchemie
Karlsruhe Institute of Technology (KIT)
Engesserstrasse 18, 76128 Karlsruhe (Germany)
N. Jasinski, Dr. A. S. Goldmann, Prof. Dr. C. Barner-Kowollik
Institut für Biologische Grenzflächen (IBG)
Karlsruhe Institute of Technology (KIT)
Herrmann-von-Helmholtz-Platz 1
76344 Eggenstein-Leopoldshafen (Germany)
Homepage: http://www.macroarc.de
Dr. D. Park
Central Facility for Electron Microscopy
RWTH Aachen University
Ahornstrasse 55, 52074 Aachen (Germany)

[**] We thank P. Das and F. Schacher for experimental help and 2D-XRD, and acknowledge financial support from the Volkswagen foundation. This work was performed in part at the Center for Chemical Polymer Technology, supported by the EU and North Rhine-Westphalia (EFRE 30 00 883 02). C.B.-K. acknowledges support from the Helmholtz BioInterfaces in Technology and Medicine as well as Science and Technology of Nanosystems programs. A.W. thanks the BMBF for support in the Aquamat Research Group and gratefully acknowledges continuous support by M. Möller.

Supporting information for this article is available on the WWW under http://dx.doi.org/10.1002/anie.201502323.

tailored supramolecular interactions, and non-autonomously self-healing materials that require energy (light, heat) to undergo self-mending. Autonomous self-healing is most attractive and requires structures with sufficient chain dynamics and/or with dynamic exchange of relatively weak supramolecular motifs, that is, hydrogen bonds. Such behavior motivates to develop, design, and understand reversible energy dissipation mechanisms in bioinspired NCs. Certainly, there has been previous work discussing hydrogen bonds in the framework of classical disordered NCs at low fractions of reinforcements.[9] For instance, McKee et al. reported on rod-like cellulose reinforcements grafted with toughening polymer chains and hydrogen bonding units. However, the final material only contained 2.5 wt% reinforcements in a disordered state.[9b]

Our focus is on self-assembled nacre mimetics at high fractions of reinforcements and with high order. Contrary to ordinary NCs, these involve nanoconfinement of the polymers into layers with periodicities typically below 3.5 nm owing to the biomimetic design principles (high inorganic content). The materials are largely defined by the interfaces, which, in combination with the nanoconfined layers, add considerable subtleness in understanding the arising properties.[4a,10] Opposed to classical high-T_g water-soluble polymers used previously,[2–6] we hypothesized that low-T_g polymers equipped with supramolecular binding motifs would keep the structure formation process as dynamic as possible to minimize structural defects, and that the amount of supramolecular units (and their type) allows the mechanical properties to be modulated in a clean and predictive way. Contrary to previous post-processing infiltration,[4b,c,6b,c,11] encoding such supramolecular units into the polymer prior to self-assembly ensures highest possible definition and characterization, required to develop quantitative structure–property relationships.

To target this challenge, we synthesized low-T_g, fully water-soluble poly(oligoethylene glycol methacrylate)-based (OEGMA) copolymers doped with different levels of 2-ureido-4-pyrimidinone (UPy) by copolymerization of OEGMA with UPy-MA (a methacrylate derivative with a UPy group) by reversible addition fragmentation transfer (RAFT) polymerization (Supporting Information, Figure S1). UPy is among the best-understood supramolecular binding motifs, and forms dimers by fourfold hydrogen bonding, as well as fibril-type aggregates due to stacking of the dimers as assisted by flanking units.[12] RAFT polymerization furnishes well-defined copolymers with similar total molecular weight ($M_n \approx 42$ kDa), low dispersity ($Đ < 1.3$), unimodal distributions, and controlled doping of UPy (Supporting Information, Table S1). The polymers are designed with moderate molecular weights, so that molecular cohesion arises from the supramolecular units rather than entanglements. We abbreviate them with EG-UPy-XX, where XX equals the molar fraction of UPy-MA (0, 13, 30 mol%). As reinforcing platelet-shaped component (Scheme 1), we utilize large-aspect-ratio synthetic sodium fluorohectorite (NHT) nanoclays, which fully delaminate in water into 1 nm thick sheets with an average aspect ratio of 750 (diameter/height; atomic force microscopy (AFM) in the Supporting Information,

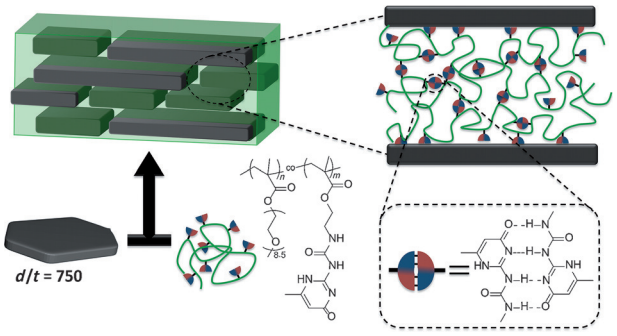

Scheme 1. Self-assembly of brick-and-mortar nacre mimetic films using high-aspect-ratio synthetic nanoclay and EG-UPy-XX. The supramolecular dimerization of the UPy motifs is depicted to the right.

Figure S2).[4a] Such synthetic high-aspect-ratio nanoclays are superior to commonly used natural montmorillonite by having a homogeneous surface charge distribution, absence of colored contaminants, and by displaying full delamination in water without problematic tactoids/aggregates.[4a,b,5,13] Hence, they could allow desirable full transparency if the structure formation is mastered and if undesirable surface defects and grain boundaries are minimized. Moreover, the high aspect ratio is appealing for flexible gas barrier applications to for example, encapsulate organic electronics.

Macroscopically, the EG-UPy-0 polymer is a viscous liquid with a $T_g \approx -61$ °C, as determined by differential scanning calorimetry (DSC). Incorporation of UPy transforms the polymers into increasingly elastic, yet still soft materials ($T_g \approx -52$ °C for EG-UPy-13, and $T_g \approx -34$ °C for EG-UPy-30). All polymers are immediately self-mending when cut or ruptured, confirming high dynamics within their structure (Supporting Information, Figure S3).

Earlier work showed that approximately a 50:50 w/w composition leads to optimum mechanical properties, allowing some inelastic deformation of the nanoconfined polymers without sacrificing stiffness.[4a,5] Therefore, we set this composition as constant. We ensured proper adhesion of the copolymers onto the nanoclay by AFM, where the thickness of the core–shell nanoplatelets (ca. 3.4 nm) is higher compared to pure NHT nanoclay (0.9 nm; Supporting Information, Figure S2). The adsorption of a single polymer layer onto the nanoclays is caused by coordination of EG units onto nanoclay and possibly assisted by adsorption of the UPy segments.[14] Such intermediately formed core–shell nanoplatelets are decisive to predefine the periodicity in the final layered NCs.

After casting, films of excellent transparency and homogeneity are obtained (Figure 1c). Such a high level of transparency is indicative of well-defined structures within the film (absence of grain boundaries), and the absence of detrimental surface defects found earlier during drying of high-aspect ratio synthetic nanoclay/polymer films.[4a] SEM indeed depicts nacre-mimetic materials with highly aligned structures across the full cross-section and with a smooth top surface (Figure 1a,b, AFM in the Supporting Information, Figure S4).

To quantify the structural periodicities and order, we conducted 1D and 2D X-ray diffraction (XRD). We find 1D

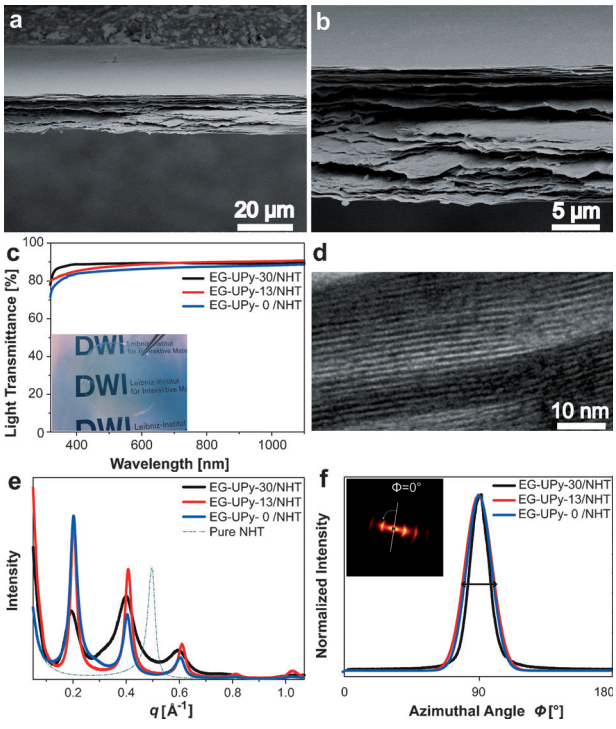

Figure 1. Structural characterization: a), b) SEM images of the cross-section of EG-UPy-13/NHT. c) Light transmittance normalized to 25 µm film thickness, including a photograph of a transparent 35 µm thick film. d) Cross-sectional TEM of EG-UPy-13/NHT with alternating hard nanoclay (dark) and soft polymer (gray) layers. e) 1D XRD of various nacre mimetics and pure NHT for comparison. f) Azimuthal intensity distribution profiles of the primary diffraction peak extracted from 2D XRD and detector image for EG-UPy-13/NHT.

diffractograms with reflections up to the eleventh integer multiple of the primary diffraction peak (Figure 1e; Supporting Information, Figure S5). This is an unusual observation for a colloidal material and clearly confirms highly aligned lamellar films with precise periodicities and long range order. Earlier nacre-mimetics mostly only showed broad first and possibly second-order diffraction peak.[4a,b,5,6c,15] The d-spacings of the lamellar structures can be calculated from the primary diffraction peak to $d \approx 3.1$ nm for all nacre mimetics, which agrees to the thickness of the polymer-coated nanoclay (ca. 3.4 nm; Supporting Information, Figure S2). TEM imaging of a focused ion beam (FIB) prepared ultrathin cross-section of EG-UPy-13/NHT confirms the alternating hard/soft layers (Figure 1d). EG-UPy-30/NHT shows a broader and comparably more intense diffraction peak in the 2q* region. This does not arise from unexfoliated clay, but likely stems from higher organization of the UPy units at higher UPy fractions.[12a,16] We quantify the degree of orientation by 2D XRD. Here, we find multiple diffraction arcs with very narrow azimuthal spreading as originating from a highly aligned mesostructure (Figure 1f). The degree of orientation Π of the nanoclay in the films can be calculated from the full width at half maximum of the peak (fwhm) according to:

$$\Pi = \frac{180-\text{fwhm})}{180}100 \qquad (1)$$

All films display a near perfect orientation in the range of 92%.

Next, we turn to the mechanical properties. Our intention was to modulate the macroscale mechanical properties by providing nanoscale, supramolecular, and reversible strengthening mechanisms by hydrogen-bonding encoded into the copolymers. Figure 2 and the Supporting Information, Table S2 summarize the tensile testing results. A fundamentally different behavior can be observed, even though only up to 30 mol% of the repeating units are exchanged to UPy. The EG-UPy-0/NHT film without any UPy shows comparably low stiffness (2 GPa) and a rather ductile behavior with strain-to-failure values around 4.4%. Directly on the other end, the 30 mol% of UPy in EG-UPy-30/NHT take a strong effect in defining the mechanical cohesion with efficient stress transfer onto the platelets, resulting in particularly stiff materials (43 GPa) with very high tensile strength (265 MPa), yet low strain-to-failure (1.3%). The lack of substantial yielding and inelastic deformation demonstrates tight cross-linking with low exchange dynamics, at least with respect to the macroscopic deformation rate (0.5 mm min^{-1}). Remarkably, this material is among the stiffest and strongest clay-based nacre-mimetic NCs ever prepared, and reaches such values at relevant relative humidity (60% RH). Tedious post-cross-linking/infiltration[4b,c,5,6b,c] is not anymore needed, as the supramolecular bonds are pre-encoded into the polymer.

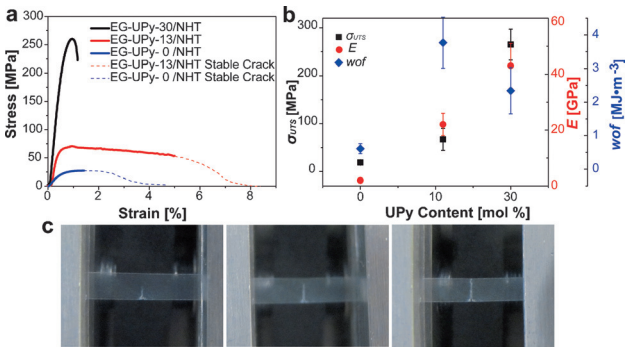

Figure 2. Mechanical tensile properties: a) Stress–strain curves, b) tensile strength (σ_{UTS}), Young's modulus (E), and work of fracture (wof) as a function of UPy content. c) Stable crack during the failure of EG-UPy-13/NHT.

EG-UPy-13/NHT takes a very interesting intermediate position. It displays a synergetic increase of the mechanical properties as compared to the material without UPy. The stiffness increases tenfold and reaches 22 GPa. At the same time, a pronounced yielding with an even longer inelastic plateau occurs. This favorably contrasts classical covalent cross-linking, for which an increase in stiffness is usually bought on the expense of strain-to-failure and toughness.[2b,4c,5,6b] Inelastic deformation goes along with frictional sliding of the nanoplatelets against each other. Hence, the higher stress level of the inelastic deformation zone upon incorporation of UPy is strongly indicative of a dynamic cross-linking scenario with stress-induced opening of supramolecular bonds and dynamic stick/slip interactions. This

behavior was suggested by simulations to target bioinspired sacrificial bonds and hidden length scales in layered materials.[7a] As a consequence, the work-of-fracture as defined by the area under the curve peaks for this composition.

Moreover, this material is remarkable in terms of fracture behavior, because, despite the high stiffness, cracks nucleate at the edges of the specimen and propagate stably and with high tortuosity during failure (Figure 2c). Importantly, this stable crack propagation is observed in a highly reinforced material (50 wt%) with high aspect ratio nanoplatelets and nanoconfined polymers, and without plasticization by submersion in water.[10] This behavior contrasts the very stiff and more brittle EG-UPy-30/NHT and displays that intermediate UPy contents are preferable to allow for simultaneous stiffening and toughening, combined with stable cracks. Such synergies are very rare and mostly less pronounced in bioinspired NCs.[6a,c] We present a detailed comparison to other nacre-mimetic nanocomposites as Ashby plot in the Supporting Information, Figure S6.

Driven by the observation of stable cracks, we investigated potential toughening and failure mechanisms by SEM. Figure 3 depicts a broad range of toughening and failure phenomena in the process zone of a EG-UPy-13/NHT NC. These are reminiscent of the behavior of highly reinforced biological materials, such as tough bone and nacre.[1c,17] The crack path shows high tortuosity with several crack branching (Figure 3a,b), crack arresting, and crack twisting phenomena (Figure 3c). Additionally, constrained microcracking occurs next to the major crack path (Figure 3d). These mechanisms indicate sufficient ability to delocalize stress away from the central crack tip owing to balanced dynamics of the soft phase and to the presence of rather large nanoclay sheets, some of which having aspect ratios of more than 10000. On the nanoscale, clear delamination and nanoclay platelet pullout can be observed (Figure 3e), again also contributing to inelastic fracture energy dissipation due to larger-scale movements in the material. Such a diverse range of nano-to-microscale toughening mechanisms has not been observed in previous clay-based nacre mimetics. For comparison, we also recorded the crack line of a material with an unstable crack (EG-UPy-30/NHT; Supporting Information, Figure S7). Therein, we find a straight crack line with limited roughness and limited platelet pullout. Hence, the dynamics in the matrix and at the matrix–nanoclay interface are unfavorably low to allow for efficient toughening mechanisms to take place if the supramolecular strengthening is in excess.

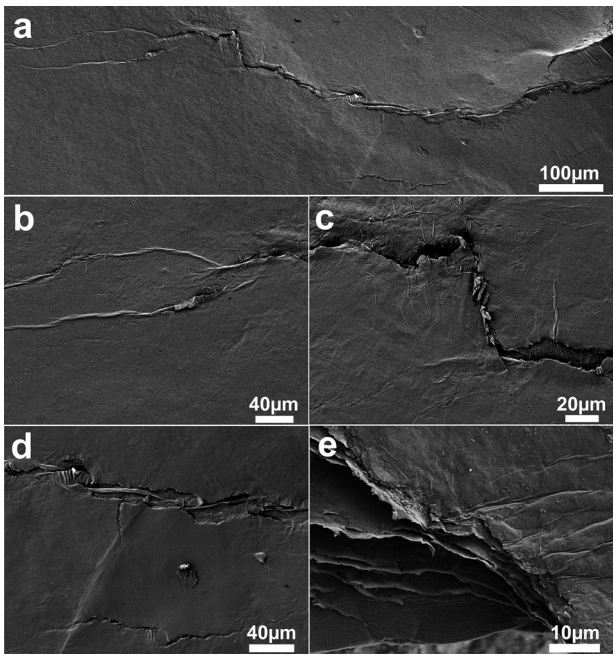

Figure 3. Toughening and failure mechanisms observed in the process zone of EG-UPy-13/NHT. a) SEM overview image of the crack tip. b) Crack branching, c) crack twisting, d) constrained microcracks formed next to major crack line and e) nanoclay platelet pullout at the crack tip.

To address multifunctional biomimetic materials with applications beyond pure mechanical performance, we discuss gas barrier properties to understand the possible suitability of the materials as flexible, transparent, and self-standing barrier materials for organic electronics. The transmittance in the visible region is about 80–90% (at 25 μm thickness), which manifests in near glass-like transparency in a photograph (Figure 1c). Nacre mimetics using natural nanoclay with similar weight fraction and thickness cannot reach such values owing to colored contamination. Previous nacre mimetics with large synthetic clays required clear coats to remove surface scattering.[4a] Hence there is a clear advantage for these materials as they can be obtained in a facile single-step procedure. For the gas-barrier properties, we focus on EG-UPy-13/NHT at high RH (80%). High RH poses challenging conditions for gas barriers based upon water-soluble polymers, as increased free volume and plasticization allow faster diffusion of gas molecules. We find an oxygen permeability of 0.013 $cc\,mm\,m^{-2}\,day^{-1}\,atm^{-1}$. This is more than one order of magnitude better than for previous nacre mimetics based on natural nanoclay.[4b] It is in range with some of the best clay-based gas barrier materials that are specifically optimized for barrier functions (mostly measured at lower RH) without attending to mechanical performance.[4a,13a,18] The combination of both is however needed to satisfy the criteria as self-standing robust film. We believe that the attractive multifunctional property profile herein can be further advanced by increasing the nanoclay aspect ratio and content.

In conclusion, we demonstrated that supramolecularly bonded, self-healing polymers allow hierarchical nacre-mimetic films with highly defined mesostructure. The mechanical properties can be largely tuned from high strain to high stiffness and strength by controlling the molecular interactions of the copolymers. Nacre mimetics with large amounts of supramolecular groups are among the stiffest and strongest ever prepared, without tedious post-cross-linking or infiltration of metal ions ($E \approx 45$ GPa, $\sigma_{UTS} \approx 270$ MPa at 60% RH). Nacre mimetics with intermediate fractions of supramolecular units display synergetic increase of stiffness, strength, and toughness, as enabled by feasible dynamics and a balance of stiffening and stress-induced opening/rebinding of supramolecular units. This efficient fracture energy dissipation yields stable cracks with multiscale toughening mechanisms

reminiscent of the role model biocomposites. Those are observed for the first time in a highly reinforced nacre mimetic with high-aspect-ratio nanoclays. Looking out to the future, the observed synergistic increase of mechanical characteristics owing to balanced dynamics and supramolecular strengthening of the soft phase, in combination with stable crack propagation, teaches first lessons for the design of advanced biomimetic NCs based on precisely engineered soft phases. We foresee further key improvements by changing the interaction strength and optimizing the segmental dynamics of the underlying polymers. Towards multifunctionality, the excellent structural control enables combinations of tunable mechanics, high transparency, and exciting gas barrier properties, rendering these films interesting for encapsulating organic electronics.

Keywords: bioinspired materials · crack propagation · nacre mimetics · sacrificial bonds · toughness

How to cite: *Angew. Chem. Int. Ed.* **2015**, *54*, 8653 – 8657
Angew. Chem. **2015**, *127*, 8777 – 8781

[1] a) J. W. C. Dunlop, P. Fratzl, *Annu. Rev. Mater. Res.* **2010**, *40*, 1 – 24; b) M. A. Meyers, P.-Y. Chen, A. Y.-M. Lin, Y. Seki, *Prog. Mater. Sci.* **2008**, *53*, 1 – 206; c) R. Z. Wang, H. S. Gupta, *Annu. Rev. Mater. Res.* **2011**, *41*, 41 – 73; d) H. B. Yao, H. Y. Fang, X. H. Wang, S. H. Yu, *Chem. Soc. Rev.* **2011**, *40*, 3764 – 3785; e) M. Suzuki, K. Saruwatari, T. Kogure, Y. Yamamoto, T. Nishimura, T. Kato, H. Nagasawa, *Science* **2009**, *325*, 1388 – 1390.

[2] a) L. J. Bonderer, A. R. Studart, L. J. Gauckler, *Science* **2008**, *319*, 1069 – 1073; b) P. Podsiadlo, A. K. Kaushik, E. M. Arruda, A. M. Waas, B. S. Shim, J. Xu, H. Nandivada, B. G. Pumplin, J. Lahann, A. Ramamoorthy, N. A. Kotov, *Science* **2007**, *318*, 80 – 83; c) H.-B. Yao, H.-Y. Fang, Z.-H. Tan, L.-H. Wu, S.-H. Yu, *Angew. Chem. Int. Ed.* **2010**, *49*, 2140 – 2145; *Angew. Chem.* **2010**, *122*, 2186 – 2191.

[3] E. Munch, M. E. Launey, D. H. Alsem, E. Saiz, A. P. Tomsia, R. O. Ritchie, *Science* **2008**, *322*, 1516 – 1520.

[4] a) P. Das, J. M. Malho, K. Rahimi, F. H. Schacher, B. Wang, D. E. Demco, A. Walther, *Nat. Commun.* **2015**, *6*, 5967; b) A. Walther, I. Bjurhager, J. M. Malho, J. Pere, J. Ruokolainen, L. A. Berglund, O. Ikkala, *Nano Lett.* **2010**, *10*, 2742 – 2748; c) A. Walther, I. Bjurhager, J. M. Malho, J. Ruokolainen, L. Berglund, O. Ikkala, *Angew. Chem. Int. Ed.* **2010**, *49*, 6448 – 6453; *Angew. Chem.* **2010**, *122*, 6593 – 6599.

[5] P. Das, S. Schipmann, J. M. Malho, B. Zhu, U. Klemradt, A. Walther, *ACS Appl. Mater. Interfaces* **2013**, *5*, 3738 – 3747.

[6] a) J. Wang, Q. Cheng, L. Lin, L. Jiang, *ACS Nano* **2014**, *8*, 2739 – 2745; b) P. Podsiadlo, A. K. Kaushik, B. S. Shim, A. Agarwal, Z. Tang, A. M. Waas, E. M. Arruda, N. A. Kotov, *J. Phys. Chem. B* **2008**, *112*, 14359 – 14363; c) L. Martikainen, A. Walther, J. Seitsonen, L. Berglund, O. Ikkala, *Biomacromolecules* **2013**, *14*, 2531 – 2535.

[7] a) M. A. Hartmann, P. Fratzl, *Nano Lett.* **2009**, *9*, 3603 – 3607; b) G. E. Fantner, T. Hassenkam, J. H. Kindt, J. C. Weaver, H. Birkedal, L. Pechenik, J. A. Cutroni, G. A. Cidade, G. D. Stucky, D. E. Morse, P. K. Hansma, *Nat. Mater.* **2005**, *4*, 612 – 616; c) E. Ducrot, Y. Chen, M. Bulters, R. P. Sijbesma, C. Creton, *Science* **2014**, *344*, 186 – 189.

[8] a) N. K. Guimard, K. K. Oehlenschlaeger, J. Zhou, S. Hilf, F. G. Schmidt, C. Barner-Kowollik, *Macromol. Chem. Phys.* **2012**, *213*, 131 – 143; b) K. K. Oehlenschlaeger, J. O. Mueller, J. Brandt, S. Hilf, A. Lederer, M. Wilhelm, R. Graf, M. L. Coote, F. G. Schmidt, C. Barner-Kowollik, *Adv. Mater.* **2014**, *26*, 3561 – 3566; c) P. Cordier, F. Tournilhac, C. Soulie-Ziakovic, L. Leibler, *Nature* **2008**, *451*, 977 – 980; d) M. D. Hager, P. Greil, C. Leyens, S. van der Zwaag, U. S. Schubert, *Adv. Mater.* **2010**, *22*, 5424 – 5430.

[9] a) R. Vaiyapuri, B. W. Greenland, H. M. Colquhoun, J. M. Elliott, W. Hayes, *Polym. Chem.* **2013**, *4*, 4902 – 4909; b) J. R. McKee, J. Huokuna, L. Martikainen, M. Karesoja, A. Nykänen, E. Kontturi, H. Tenhu, J. Ruokolainen, O. Ikkala, *Angew. Chem. Int. Ed.* **2014**, *53*, 5049 – 5053; *Angew. Chem.* **2014**, *126*, 5149 – 5153; c) C.-C. Peng, A. Göpfert, M. Drechsler, V. Abetz, *Polym. Adv. Technol.* **2005**, *16*, 770 – 782.

[10] T. Verho, M. Karesoja, P. Das, L. Martikainen, R. Lund, A. Alegria, A. Walther, O. Ikkala, *Adv. Mater.* **2013**, *25*, 5055 – 5059.

[11] P. Das, A. Walther, *Nanoscale* **2013**, *5*, 9348 – 9356.

[12] a) W. P. J. Appel, G. Portale, E. Wisse, P. Y. W. Dankers, E. W. Meijer, *Macromolecules* **2011**, *44*, 6776 – 6784; b) M. Hutin, E. Burakowska-Meise, W. P. J. Appel, P. Y. W. Dankers, E. W. Meijer, *Macromolecules* **2013**, *46*, 8528 – 8537; c) H. Kautz, D. J. M. van Beek, R. P. Sijbesma, E. W. Meijer, *Macromolecules* **2006**, *39*, 4265 – 4267.

[13] a) M. W. Möller, T. Lunkenbein, H. Kalo, M. Schieder, D. A. Kunz, J. Breu, *Adv. Mater.* **2010**, *22*, 5245 – 5249; b) N. Miyamoto, H. Iijima, H. Ohkubo, Y. Yamauchi, *Chem. Commun.* **2010**, *46*, 4166 – 4168.

[14] A. Nelson, T. Cosgrove, *Langmuir* **2004**, *20*, 2298 – 2304.

[15] a) A. K. Kaushik, P. Podsiadlo, M. Qin, C. M. Shaw, A. M. Waas, N. A. Kotov, E. M. Arruda, *Macromolecules* **2009**, *42*, 6588 – 6595; b) W. Cui, M. Z. Li, J. Y. Liu, B. Wang, C. Zhang, L. Jiang, Q. F. Cheng, *ACS Nano* **2014**, *8*, 9511 – 9517; c) J. J. Kochumalayil, M. Bergenstrahle-Wohlert, S. Utsel, L. Wagberg, Q. Zhou, L. A. Berglund, *Biomacromolecules* **2013**, *14*, 84 – 91; d) L. Q. Liu, Y. Gao, Q. Liu, J. Kuang, D. Zhou, S. T. Ju, B. H. Han, Z. Zhang, *Small* **2013**, *9*, 2466 – 2472; e) A. Liu, A. Walther, O. Ikkala, L. Belova, L. A. Berglund, *Biomacromolecules* **2011**, *12*, 633 – 641.

[16] J. L. Wietor, D. J. M. van Beek, G. W. Peters, E. Mendes, R. P. Sijbesma, *Macromolecules* **2011**, *44*, 1211 – 1219.

[17] R. K. Nalla, J. H. Kinney, R. O. Ritchie, *Nat. Mater.* **2003**, *2*, 164 – 168.

[18] a) T. Ebina, F. Mizukami, *Adv. Mater.* **2007**, *19*, 2450 – 2453; b) M. W. Möller, D. A. Kunz, T. Lunkenbein, S. Sommer, A. Nennemann, J. Breu, *Adv. Mater.* **2012**, *24*, 2142 – 2147; c) M. A. Priolo, D. Gamboa, J. C. Grunlan, *ACS Appl. Mater. Interfaces* **2010**, *2*, 312 – 320.

Received: March 12, 2015
Published online: June 10, 2015

